nature structural & molecular biology

Histone H2A.Z inheritance during the cell cycle and its impact on promoter organization and dynamics

Maxim Nekrasov[1], Jana Amrichova[1,3], Brian J Parker[1,3], Tatiana A Soboleva[1], Cameron Jack[1], Rohan Williams[1,2], Gavin A Huttley[1] & David J Tremethick[1]

Although it has been clearly established that well-positioned histone H2A.Z–containing nucleosomes flank the nucleosome-depleted region (NDR) at the transcriptional start site (TSS) of active mammalian genes, how this chromatin-based information is transmitted through the cell cycle is unknown. We show here that in mouse trophoblast stem cells, the amount of histone H2A.Z at promoters decreased during S phase, coinciding with homotypic (H2A.Z–H2A.Z) nucleosomes flanking the TSS becoming heterotypic (H2A.Z–H2A). To our surprise these nucleosomes remained heterotypic at M phase. At the TSS, we identified an unstable heterotypic histone H2A.Z–containing nucleosome in G1 phase that was lost after DNA replication. These dynamic changes at the TSS mirror a global expansion of the NDR at S and M phases, which, unexpectedly, is unrelated to transcriptional activity. Coincident with the loss of histone H2A.Z at promoters, histone H2A.Z is targeted to the centromere when mitosis begins.

The incorporation of variant histones into chromatin is important in establishing an active transcriptionally poised chromatin structure encompassing the TSS[1]. Studies have indicated that the TSS of active genes transcribed by RNA polymerase II are depleted in stable nucleosomes to create an NDR, which is believed to be necessary for the binding of transcription machinery[2–4]. Although the mechanism(s) that control the size and the location of the NDR is poorly understood, it is established that the NDR is flanked on both sides by histone H2A.Z–containing nucleosomes in mammalian cells[5,6]. Notably, the TSS of an active gene is not nucleosome-free but comprises a labile histone H3.3–H2A.Z double-variant nucleosome[7]. These double-variant nucleosomes also mark CTCF insulator binding factor sites[7]. Despite these nucleosomes being highly unstable and dynamic[8], a structural explanation for this lability is missing[9].

At a cellular level, the structure and composition of chromatin at the promoter has a fundamental role in maintaining cell states, especially in undifferentiated stem cells, by ensuring that gene expression patterns are stably inherited from one cell generation to the next[10]. For transmission of this chromatin-based information during cell division, this information must be restored after the highly disrupting process of DNA replication (S phase) and remain with chromosomes as they condense during metaphase (M phase). Unlike canonical histones, histone H2A.Z is expressed throughout the cell cycle[11] (**Supplementary Fig. 1a**). However, how the histone H2A.Z–containing nucleosomes that flank the TSS, and the NDR itself, are inherited is unknown.

RESULTS

Less histone H2A.Z at promoters after DNA replication

Given the importance of understanding how the chromatin structure of an active gene is inherited during the cell cycle, we determined how histone H2A.Z is transmitted after DNA replication and then maintained at active promoters during the onset of M phase[6]. To do this, we used mouse trophoblast stem cells as a model system, given that histone H2A.Z is required for their viability[12]. We synchronized trophoblast stem cells at the G1-S, G2-M and S phase boundaries (Online Methods and **Supplementary Fig. 2**). We then performed histone H2A.Z chromatin immunoprecipitation followed by high-throughput sequencing (ChIP-seq) experiments and examined global gene expression using whole mouse genome expression microarrays at these three stages of the cell cycle (**Fig. 1a–c**).

We separated ~18,000 mouse genes into ~180 groups of 100 genes according to their expression level (**Fig. 1**). For each group of 100 genes, a single line represents the normalized tag counts at each base pair, which has been aligned with the TSS (±1 kb) for protein-coding genes. The color map (**Fig. 1a**) shows the relationship between color and the gene expression rank for a group of genes. As has been reported before[5], there is an apparent positive correlation between the level of transcription and the presence of histone H2A.Z at the promoter for genes expressed at G1, S and M phases (**Fig. 1a–c**). The two histone H2A.Z–containing nucleosomes positioned on either side of the TSS (at nucleosome positions −2 and +1 with the TSS being the −1 position) are a hallmark of active promoters in mammalian cells[5]. We also observed a gradual loss of the +1 histone H2A.Z–containing

[1]The John Curtin School of Medical Research, The Australian National University, Canberra, Australian Capital Territory, Australia. [2]Present address: Singapore Centre on Environmental Life Sciences Engineering, National University of Singapore, Singapore. [3]These authors contributed equally to this work. Correspondence should be addressed to D.J.T. (david.tremethick@anu.edu.au).

Received 26 June; accepted 24 September; published online 21 October 2012; doi:10.1038/nsmb.2424

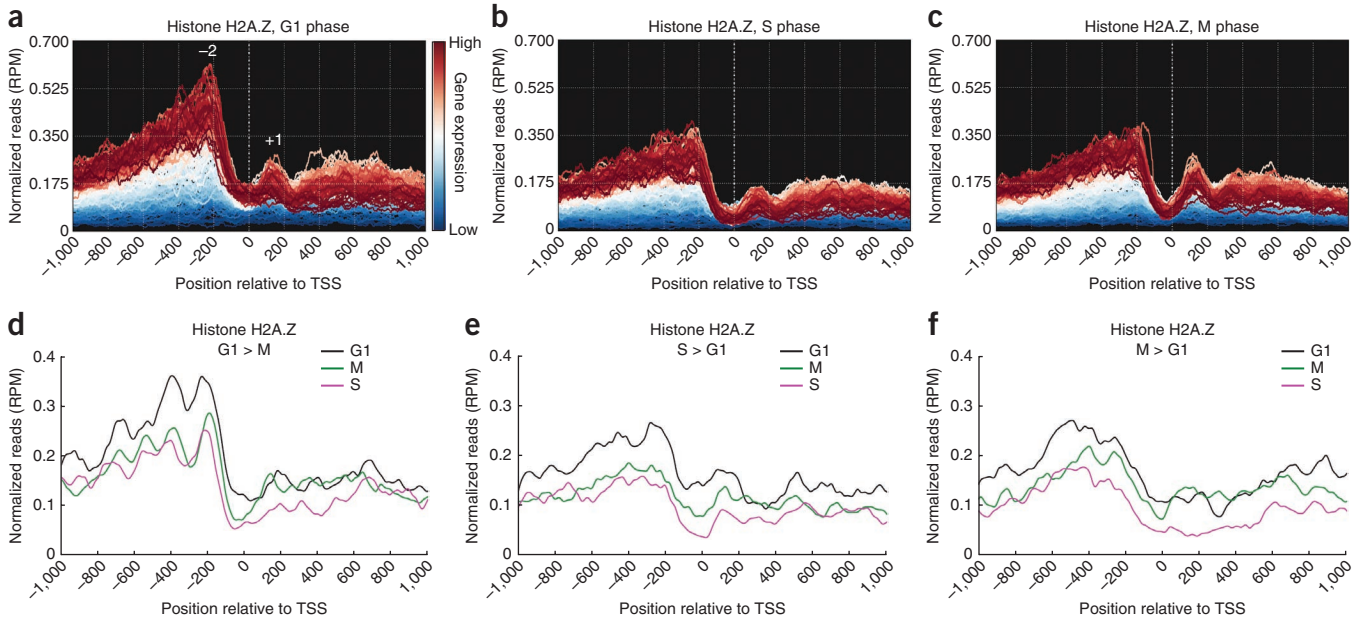

Figure 1 The amount of histone H2A.Z present at active promoters is cell cycle–dependent. (**a**) Histone H2A.Z ChIP-seq experiments and a global gene expression analysis in trophoblast stem (TS) cells at G1 phase; 179 H2A.Z ChIP profiles were generated. Each line represents a group of 100 genes and represents the normalized tag counts at each base pair (reads per million (RPM) mapped), aligned between −1 kb and +1 kb from the TSS. The line color reflects the average gene expression rank of the 100 genes. The color map shows the relationship between color and the gene expression rank. Histone H2A.Z nucleosomes positioned immediately upstream (−2) and downstream (+1) of the TSS are shown. (**b**) Histone H2A.Z ChIP-seq experiments and a global gene expression analysis in TS cells at S phase. Histone H2A.Z normalized tag counts for 177 groups of 100 genes aligned with the TSS are shown. (**c**) Histone H2A.Z ChIP-seq experiments and a global gene expression analysis in TS cells at M phase. H2A.Z normalized tag counts for 179 groups of 100 genes aligned with the TSS are shown. (**d**–**f**) Top 100 differentially expressed genes for G1 phase greater than M phase (G1 > M; **d**), S phase greater than G1 phase (S > G1; **e**) and M phase greater than G1 phase (M > G1; **f**) represented as a single line of normalized H2A.Z counts at each base pair, aligned with the TSS.

nucleosome as well as of histone H2A.Z–containing nucleosomes farther downstream for the highest-expressing groups of genes, indicating transcription-mediated displacement of histone H2A.Z (**Fig. 1a**). To our surprise, however, the normalized histone H2A.Z tag count was reduced across the promoter region for genes active in S and M phases compared to genes expressed in G1 phase.

To distinguish whether this reduction in the amount of histone H2A.Z was due to a general loss of histones from active promoters at S and M phases or a specific loss of histone H2A.Z, we performed histone H3 ChIP-seq experiments and determined the loss of histone H2A.Z relative to that of histone H3 (**Supplementary Fig. 3**). There was clear, specific loss of histone H2A.Z, demonstrating that promoters that are active at S and M have less histone H2A.Z than promoters active at G1 phase (**Supplementary Fig. 3d**–**f**).

We then investigated whether the reduced amounts of histone H2A.Z for genes expressed at S and M phases are related to transcription levels at these stages of the cell cycle or whether they are an indirect consequence of the disruption of chromatin that occurs during DNA replication at S phase. To do this, we identified genes whose expression was significantly upregulated or downregulated ($P < 0.01$) in G1 versus M, S versus G1 and S versus M phases, and compared their relative expression (**Supplementary Fig. 4**). We found that the relative expression levels of genes expressed at S and M phases were similar to those genes expressed at G1 phase (**Supplementary Fig. 4a**,**d**). We then chose the top 100 differentially expressed genes for G1 phase greater than M phase (G1 > M), S phase greater than G1 phase (S > G1) and M phase greater than G1 phase (M > G1), and represented them as a single line of normalized histone H2A.Z tag counts at each base pair, aligned with the TSS (**Fig. 1d**–**f**). We then examined changes in these profiles as the trophoblast stem cells cycle from G1 phase to M phase.

Unexpectedly, for all groups of genes, whether they were more highly expressed at G1, S or M phase, the overall highest normalized histone H2A.Z tag count occurred at G1 phase (**Fig. 1d**–**f**). These results argue that the amount of histone H2A.Z at active promoters is cell cycle–dependent, which is highlighted by the observation that for genes that are more highly expressed at S or M phases versus G1 phase, their promoter regions contain more histone H2A.Z at G1 phase (**Fig. 1e**,**f**). To test the proposal that the amount of promoter-bound histone H2A.Z decreases after S phase, we examined the highest 100 expressed housekeeping genes that display no major changes in gene expression between G1 phase, and S and M phases of the cell cycle. Despite the expression not changing between the different stages of the cell cycle, the overall highest normalized histone H2A.Z tag count at the promoter also occurred at G1 phase (**Supplementary Fig. 5a**).

To validate our interpretation of the ChIP-seq data that the amount of histone H2A.Z is reduced at active promoters after the passage through S phase, we performed quantitative histone H2A.Z ChIP assays examining the relative amount of histone H2A.Z at the −2 and +1 nucleosome, and at the TSS of genes either expressed at G1 phase (*Liph*, *Cdh5* and *Esam*) or at M phase (*Skap2*, *Plk1* and *Zic5*) (genes were chosen from the top 100 differentially expressed genes for G1 > M and M > G1, respectively; **Fig. 2** and **Supplementary Fig. 6**). For all of these active genes, irrespective of when they are expressed, the highest level of histone H2A.Z at all three promoter locations occurred in G1 phase (**Fig. 2a**,**b**). Notably, the reduction of histone H2A.Z at M phase was not cell type–specific because we also observed a similar reduction in amounts of histone H2A.Z in human U20S cells (**Fig. 2c**,**d**). Taken together, we conclude that although there is a

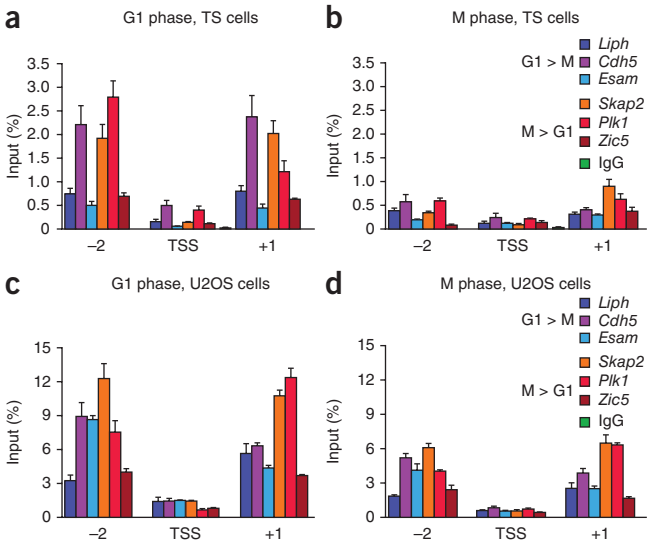

Figure 2 Genes that are more highly expressed at M phase have more histone H2A.Z at their promoters in G1 phase. (**a**–**d**) Histone H2A.Z at the –2 and +1 nucleosome positions and at the TSS for genes expressed at G1 (*Liph*, *Cdh5* and *Esam*) or M (*Skap2*, *Plk1* and *Zic5*) phases in trophoblast stem (TS) cells (**a**,**b**) or U2OS cells (**c**,**d**) determined by quantitative histone H2A.Z ChIP assays performed at G1 phase (**a**,**c**) or M phase (**b**,**d**). The amount of histone H2A.Z ChIP DNA was determined as a percentage of input DNA using quantitative PCR. Error bars, s.d. ($n = 6$ for **a**,**b**; $n = 3$ for **c**,**d**).

positive correlation between transcription and the accumulation of histone H2A.Z at the promoter within each individual stage of the cell cycle (**Fig. 1a**–**c**), no such correlation exists between the different stages of the cell cycle because for all active genes examined, the highest histone H2A.Z content occurred at G1 phase (**Figs. 1** and **2**). In other words, there appears to be a global loss of histone H2A.Z at the promoter after S phase. Moreover, these results imply that transcription of M phase–specific genes was not affected by lower levels of histone H2A.Z (**Fig. 2** and **Supplementary Fig. 6**).

Why is histone H2A.Z not fully restored at promoters after S phase to G1-phase amounts? Histone H2A.Z is expressed throughout the cell cycle with no major increase in expression at S phase[11] (**Supplementary Fig. 1a**), and therefore, there may be simply insufficient histone H2A.Z to double its absolute nucleosomal content after the passage of the replication fork. To determine whether this is the case, we performed a western blot analysis using the same input chromatin as that used for histone H2A.Z ChIP-seq experiments (**Fig. 1**). We then determined the amount of histone H2A.Z in these chromatin preparations relative to that of histone H3 at G1, S and M phases (**Supplementary Fig. 1b**). Contrary to our expectation, we observed no change in the amount of chromatin-bound histone H2A.Z, relative to that of histone H3, at different stages of the cell cycle. This indicates that the depletion of histone H2A.Z at promoters after S phase cannot be simply explained by the dilution of histone H2A.Z during and after DNA replication.

Figure 3 Heterotypic histone H2A.Z–H2A nucleosomes are assembled after S phase. (**a**) Schematic of the experiment: ChIP assays were first performed using affinity purified anti–histone H2A.Z antibodies to immunoprecipitate all histone H2A.Z-containing nucleosomes followed by a second ChIP using anti–histone H2A antibodies to pull down heterotypic nucleosomes. For the ChIP histone H2A.Z reChIP histone H2A experiments, the original ChIP H2A.Z material served as input DNA. A, histone H2A; Z, histone H2A.Z. (**b**) The amount of histone H2A.Z reChIP H2A DNA was determined relative to the original amount of histone H2A.Z ChIP DNA (blue), normalized to 100%, for each of the three stages of the cell cycle. Mean ± s.e.m. ($n = 6$) were: for G1 phase, 6.76 ± 1.15; for S phase, 5.11 ± 0.50; and for M phase, 35.2 ± 3.96.

Heterotypic histone H2A.Z–H2A nucleosomes form after S phase

Next we addressed how histone H2A.Z-containing nucleosomes are inherited after S phase especially considering the loss of histone H2A.Z at the promoter: would there be an increase in heterotypic (H2A.Z–H2A) nucleosomes or would the ratio of heterotypic (H2A.Z–H2A) to homotypic (H2A.Z–H2A.Z) nucleosomes remain unchanged after S phase? We performed histone H2A.Z ChIP assays using affinity-purified anti–histone H2A.Z antibodies to immunoprecipitate all histone H2A.Z–containing nucleosomes followed by a second ChIP (re-ChIP) using anti–histone H2A antibodies to pull down heterotypic nucleosomes. Then we determined the amount of histone H2A.Z reChIP histone H2A DNA relative to the original amount of histone H2A.Z ChIP DNA at each of the three stages of the cell cycle (**Fig. 3**).

We observed that only ~5% of histone H2A.Z nucleosomes at G1 were heterotypic, but by M phase, this dramatically increased to ~35% (**Fig. 3**). Therefore, the ratio of heterotypic (H2A.Z–H2A) to homotypic (H2A.Z–H2A.Z) nucleosomes was cell cycle–dependent. To investigate whether heterotypic nucleosomes form at active promoters after S phase, we used the same gene expression analysis as that used in the experiments described in **Figure 1** to produce a histone H2A.Z reChIP histone H2A profile for the three stages of the cell cycle; for each of the ~180 groups of 100 genes, a single line represents the normalized tag counts at each base pair, which has been aligned with the TSS (±1 kb) for protein-coding genes (**Fig. 4a**–**c**).

Notably, heterotypic histone H2A.Z nucleosomes existed at G1 phase on active promoters, but these heterotypic nucleosomes were located primarily at the TSS (**Fig. 4a**). Genes expressed at S and M phases exhibited several new features not observed for genes expressed at G1 phase (**Fig. 4b**,**c**). First, the histone H2A.Z–H2A nucleosome at the TSS was lost both at S and M phases. Second, there was a clear increase in amounts of histone H2A.Z–H2A nucleosomes upstream of the TSS. Downstream of the TSS, regularly spaced heterotypic nucleosomes appeared (a spacing of ~200 base pairs) with their abundance decreasing with increasing transcriptional activity, indicating that these nucleosomes are also disrupted in a transcription-dependent manner. Most notable was the appearance of a heterotypic nucleosome at the +1 position for genes expressed at S and M phases but not at G1 phase.

To confirm that there is an increase of histone H2A.Z–H2A nucleosomes at active promoters after S phase, we took the same

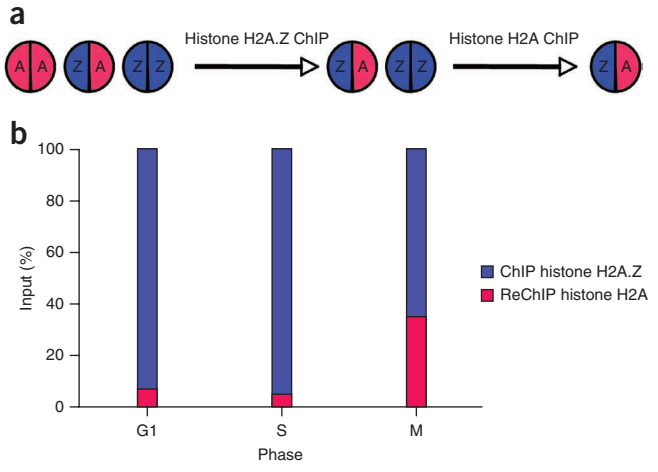

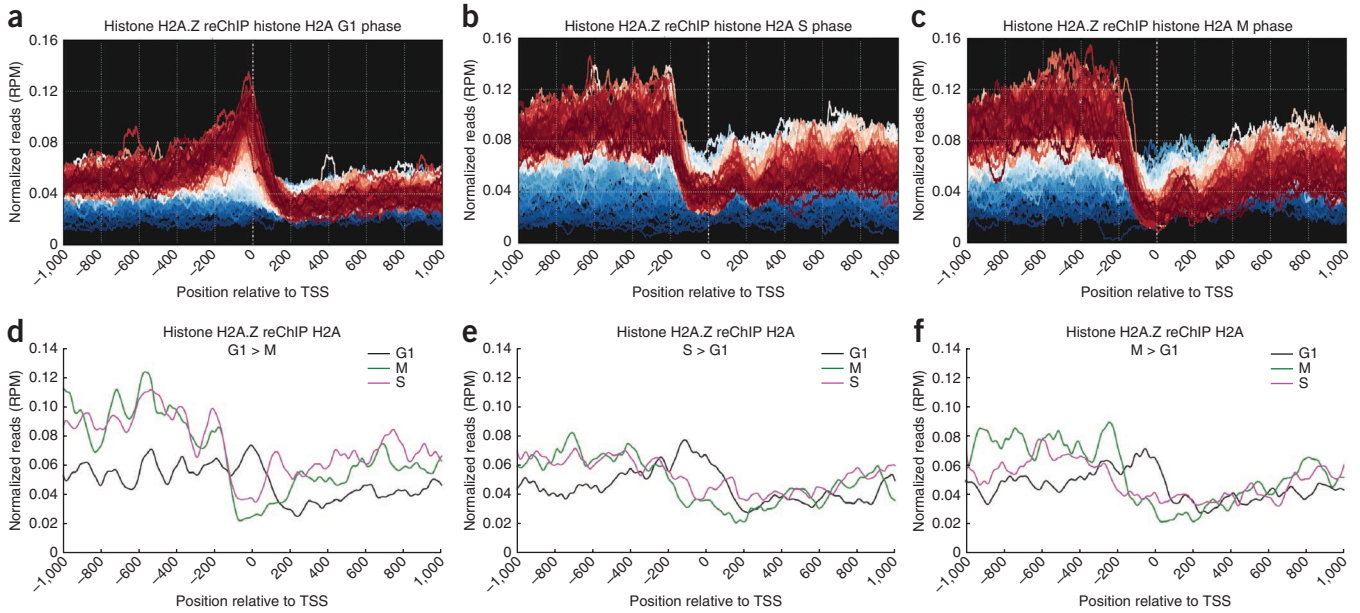

Figure 4 A heterotypic histone H2A.Z–H2A nucleosome occupies the TSS but only at G1 phase. (**a**) Histone H2A.Z ChIP–histone H2A reChIP profiles (179 profiles) were generated for the G1 phase. Each individual line represents a group of 100 genes and represents the normalized tag counts at each base pair, aligned between −1 kb and +1 kb from the TSS. The line color reflects the average gene expression rank of the 100 genes as in **Figure 1**. (**b**) Histone H2A.Z ChIP–histone H2A reChIP normalized tag counts at S phase for 177 groups of 100 genes aligned with the TSS. (**c**) Histone H2A.Z normalized tag counts at M phase for 179 groups of 100 genes aligned with the TSS. (**d**) Histone H2A.Z ChIP– histone H2A reChIP profiles of the top 100 G1 > M differentially expressed genes as in **Figure 1**. (**e**) Histone H2A.Z ChIP–histone H2A reChIP profiles of the top 100 S > G1 differentially expressed genes. (**f**) Histone H2A.Z ChIP–histone H2A reChIP profiles of the top 100 M > G1 differentially expressed genes.

top 100 differentially expressed genes as used above (**Fig. 1d–f**) for G1 > M, S > G1 and M > G1, and represented them as a single line of normalized histone H2A.Z reChIP histone H2A tag counts at each base pair, aligned with the TSS (**Fig. 4d–f**). For all groups of genes, whether they are preferentially expressed at G1, S or M phases, a histone H2A.Z–H2A heterotypic nucleosome was present at the TSS at G1 phase but was displaced at S phase and remained evicted at M phase. For G1 > M expressed genes, there was a clear increase in histone H2A.Z reChIP histone H2A signal both upstream and downstream of the TSS at S and M phases compared to that G1 phase (**Fig. 4d**). We also observed this increase of histone H2A.Z–H2A heterotypic nucleosomes upstream of the TSS for genes preferentially expressed at S and M phases (**Fig. 4e,f**). This increase was less marked downstream of the TSS perhaps as a consequence of the transcription process as noted above.

We conclude that coincident with the decrease of histone H2A.Z at active promoters (**Figs. 1** and **2**), there was an increase in nucleosomes containing both histone H2A.Z–H2A during and after S phase (**Fig. 4**). This increase in histone H2A.Z–H2A nucleosomes at the promoter was not correlated with transcription because irrespective of when these groups of genes were more highly expressed, they all displayed the same cell cycle–dependent changes. In other words, the passage through S phase leads to the changes in abundance and composition of histone H2A.Z–containing nucleosomes. Notably, the formation of the histone H2A.Z–H2A heterotypic nucleosome at the TSS is also not correlated with transcriptional activity, which raises the question of the function of the heterotypic nucleosome.

G1 phase–specific histone H2A.Z–H2A heterotypic nucleosomes

Previously it has been shown that the micrococcal sensitive nucleosome that marks the TSS comprises two histone variants, H3.3 and H2A.Z (ref. 7). We found here that this labile nucleosome is also heterotypic with respect to histone H2A.Z for genes active at G1 phase (**Fig. 4**). We therefore wondered whether other known histone H3.3–H2A.Z nucleosome-binding sites are also marked by a heterotypic histone H2A.Z–H2A nucleosome. Previously it has been shown that this double variant nucleosome also occupies CTCF insulator binding sites[7].

We produced histone H2A.Z ChIP histone H2A reChIP profiles showing normalized tag counts at each base pair aligned between −1 kilobase (kb) and +1 kb from CTCF binding sites based on Encode mouse CTCF ChIP-seq data (CTCF binding has been shown to be largely common between different cell types[13]) (**Fig. 5a** and Online Methods). Indeed, a histone H2A.Z–H2A heterotypic nucleosome is also located at CTCF insulator binding sites at G1 phase. Therefore, we suggest that a hallmark of these double-variant nucleosomes is that they contain only one histone H2A.Z. Moreover, the loss of histone H2A.Z–H2A heterotypic nucleosome present at G1 phase may be universal because this nucleosome is also displaced from CTCF binding sites during S phase and remains absent at M phase (**Fig. 5a**). We obtained identical results when we examined DNaseI-hypersensitive sites, which are also marked by these double variant–containing nucleosomes (data not shown).

To address how this loss of a histone H2A.Z–H2A nucleosome affects CTCF binding itself, we performed CTCF ChIP-seq experiments at the different stages of the cell cycle (**Fig. 5b**). In agreement with the Encode mouse CTCF ChIP-seq data used in **Figure 5a**, we observed a strong peak of CTCF protein binding matching the location of the histone H2A.Z–H2A heterotypic nucleosome at the CTCF binding site. However, notable cell-cycle differences in binding were evident (**Fig. 5b**). At G1 phase, we observed a broad and symmetrical binding pattern comprising three apparent binding peaks. One binding peak was centered at the CTCF binding site, whereas the other two

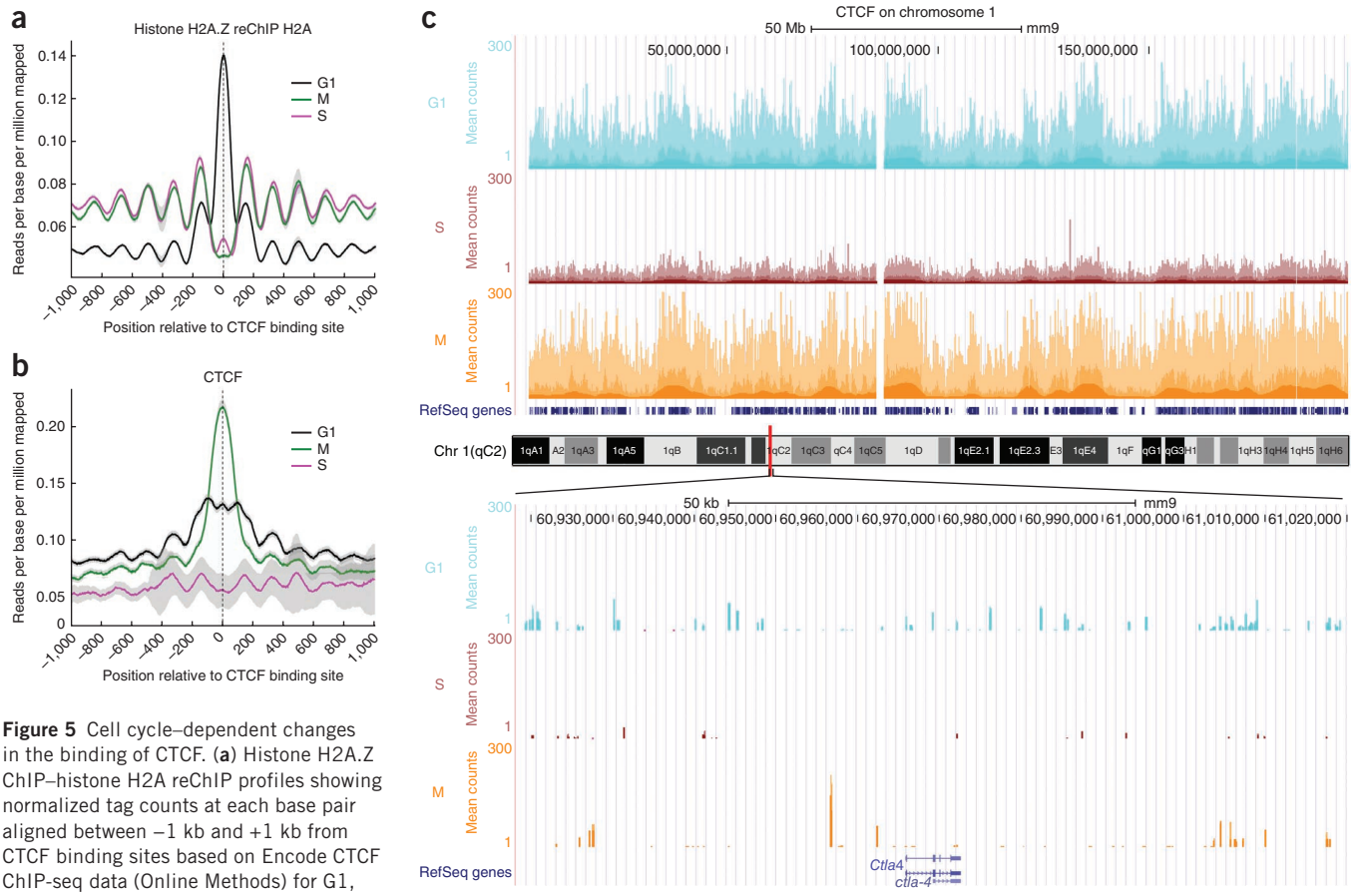

Figure 5 Cell cycle–dependent changes in the binding of CTCF. (**a**) Histone H2A.Z ChIP–histone H2A reChIP profiles showing normalized tag counts at each base pair aligned between −1 kb and +1 kb from CTCF binding sites based on Encode CTCF ChIP-seq data (Online Methods) for G1, S and M phase cells. (**b**) CTCF ChIP profiles showing normalized tag counts at each base pair (normalized per million mapped reads; RPM) aligned between −1 kb and +1 kb from CTCF binding sites based on Encode CTCF ChIP-seq data for G1, S and M phase cells. Gray banding shows a 95% confidence interval at each base pair. (**c**) Coverage of CTCF ChIP-seq reads mapped to chromosome 1 from cells in G1, S and M phase. Below is a region of chromosome 1 zoomed in to show the changes in CTCF binding between G1 and M phase cells. Mouse reference genome used was version NCBI37 mm9.

sites of binding were located ~100 base pairs upstream and downstream, respectively, from the central binding site. During S phase, CTCF protein binding is lost but is restored at M phase. In M phase, when the histone H2A.Z–H2A heterotypic nucleosome is displaced (**Fig. 5a**), we observed only one major peak of binding centered at the CTCF binding site (**Fig. 5b**). We therefore conclude that the loss of the heterotypic histone H2A.Z–containing nucleosome at M phase does impact how CTCF protein interacts with its binding site.

To investigate whether the location of CTCF binding sites changed during the cell cycle, we examined the coverage of CTCF ChIP-seq reads mapped to chromosome 1 at G1, S and M phases (**Fig. 5c**). Many of the binding sites that existed at G1 phase were no longer present at M phase and vice versa (**Fig. 5c**). Our analysis of chromosome 1 revealed that 63% of the CTCF binding sites present at M phase were not found at G1 phase (Online Methods). Based on the function of CTCF[14], our results indicate that major changes in the organization of the genome occur as the trophoblast stem cell cycles between G1 and M phases.

Histone H2A.Z is targeted to the centromere at M phase

One possible explanation for the depletion of H2A.Z at promoters after S phase is that it is targeted or redistributed to other regions of the genome. Histone H2A.Z has a second important role, which is to keep the genome stable by organizing the centromere and surrounding constitutive heterochromatin into a specialized 3D structure required for chromosome segregation at anaphase[15,16]. We therefore wondered whether there is a specific cell cycle–dependent increase in amounts of histone H2A.Z at constitutive heterochromatin (comprising major satellite DNA) and/or at the centromere (comprising minor satellite DNA).

Previously, we have used the ChIP assay to demonstrate that histone H2A.Z is associated with both major and minor satellite DNA[15]. We immunoprecipitated histone H2A.Z–containing nucleosomes at G1, S and M phases; after we generated and normalized ChIP-seq libraries to the same DNA concentration, we analyzed the libraries by quantitative PCR using specific primers for these different repetitive DNA elements. To investigate other repetitive DNA sequences, we examined subtelomeric regions and long interspersed elements (LINEs).

There was a ~45-fold and ~12-fold increase in the amount of histone H2A.Z at the centromere and subtelomeric regions, respectively, as trophoblast stem cells cycled from G1 phase to M phase (**Fig. 6a**). In contrast, there was no increase in the amount of histone H2A.Z at constitutive heterochromatin or LINEs. Therefore, in contrast to the loss of histone H2A.Z at promoters, there was a major targeting of histone H2A.Z to the centromere at a time when it becomes functionally important. The M phase–specific enrichment of histone H2A.Z at subtelomeric regions may be a new function for this histone variant.

Next, we investigated whether this increase in the amount of histone H2A.Z at the centromere and subtelomeric region is the result of an increase in the amount of histone H2A.Z–containing

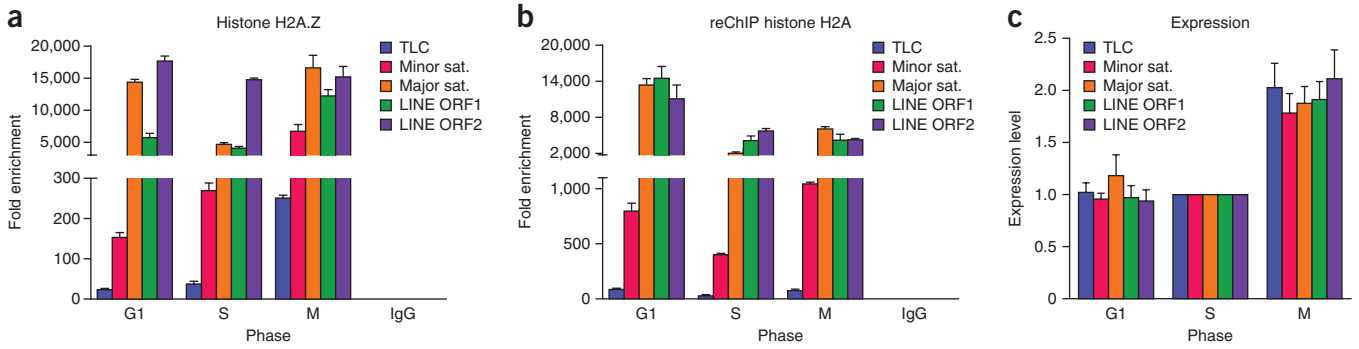

Figure 6 Targeting of histone H2A.Z to the centromere at M phase. (**a**) Quantitative PCR of normalized ChIP-seq libraries of histone H2A.Z–containing nucleosomes immunoprecipitated at G1, S or M phases. Input nucleosomes were also immunoprecipitated with IgG and analyzed as a control. Enrichment at subtelomeric regions (TLC), centromeres (minor sat.), constitutive heterochromatin (major sat.), LINE 1 open reading frame 1 (LINE ORF1) and LINE 1 open reading frame 2 (LINE ORF2) was analyzed. (**b**) Quantitative PCR of the same regions as in **a** of ChIP-seq libraries of nucleosomes containing heterotypic histone H2A.Z–H2A immunoprecipitated at G1, S or M phases. (**c**) RNA expression for each of the five different repetitive DNA elements was determined at G1, S and M phases by quantitative PCR normalized to that during S phase. Error bars, s.d. ($n = 6$).

nucleosomes that were either homotypic or heterotypic. To answer this question, we performed histone H2A.Z ChIP histone H2A reChIP experiments (**Fig. 6b**). In contrast to the major increase in amounts of histone H2A.Z at these genomic locations, we observed no such increase for histone H2A.Z–H2A heterotypic nucleosomes, demonstrating that the increase in amounts of histone H2A.Z at subtelomeric and centromeric regions was in the form of homotypic histone H2A.Z–containing nucleosomes (**Fig. 6b**). This increase in amounts of histone H2A.Z at the centromere and subtelomeric region appears not to be related to transcription because all repeated regions showed only a modest increase in transcription at M phase relative to S phase (**Fig. 6c**), supporting our previous conclusion that histone H2A.Z has an important structural role in organizing the centromere[15]. We conclude that there is a cell cycle–dependent increase in amounts of histone H2A.Z at repetitive DNA elements that are crucial for chromosome stability.

The size of the NDR increases during S phase

What controls the size and location of the NDR at the TSS is poorly understood. Given the observed cell-cycle changes in amounts of histone H2A.Z at the TSS, we investigated whether there are any alterations to the NDR. To do this, we examined nucleosome occupancy for genes more highly expressed at G1, S and M phases by sequencing input nucleosomes that we used for the above H2A.Z ChIP-seq experiments (**Fig. 7**). We aligned these reads to the TSS according to the expression rank of the same ~180 groups of 100 genes as used in **Figures 1** and **3**. We note that this analysis does not reveal the phased nucleosomes near the TSS of active genes that has been reported

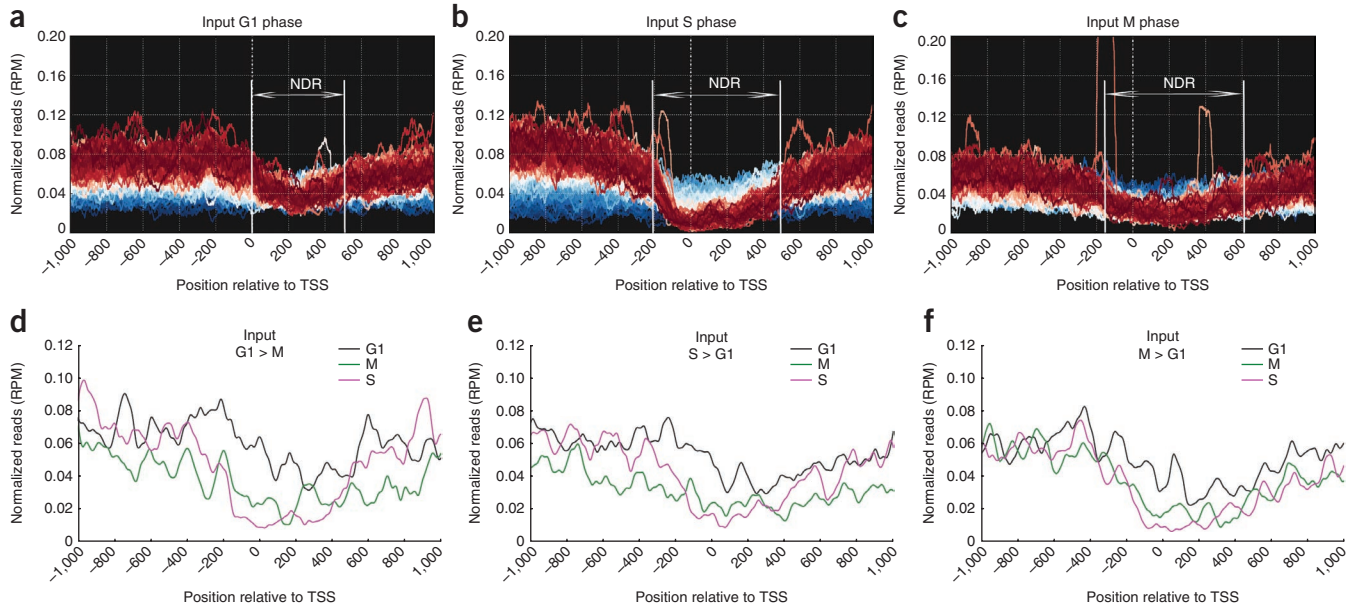

Figure 7 A dramatic expansion of the NDR for genes expressed at S and M phases compared to G1 phase–expressed genes. (**a**–**f**) Input nucleosomes were sequenced and combined with the same global gene expression analysis at the G1, S, and M stages of the cell cycle as described in **Figure 1**. Sequenced input nucleosomes for the same 179 groups of 100 genes as in **Figure 1a** (**a**). Sequenced input nucleosomes for the same 177 groups of 100 genes as in **Figure 1b** (**b**). Sequenced input nucleosomes for the same 179 groups of 100 genes as in **Figure 1c** (**c**). Vertical white lines show the increase in the size of the NDR at S and M phases compared to G1 phase. Input nucleosome profiles for the same G1 > M genes as in **Figure 1d** (**d**). Input nucleosome profiles for the same S > G1 genes as in **Figure 1e** (**e**). Input nucleosome profiles for the same M > G1 genes as in **Figure 1f** (**f**).

previously[17] because of the relatively small number of genes per group we use here (100 genes per group) as we observed phasing using more genes (~4,500 genes per group; **Supplementary Fig. 7a**).

Notably, for genes active at G1 phase, the TSS was occupied by a stable nucleosome (which is positively correlated with transcription; **Supplementary Fig. 7a** and **Fig. 7a**) and thus is not nucleosome-free as has been reported previously for asynchronously growing cells[17]. The micrococcal nuclease–sensitive NDR was instead located ~220 base pairs downstream of the TSS (**Fig. 7a** and **Supplementary Fig. 7b**). The size of this NDR dramatically increased for genes expressed both at S phase and at M phase (**Fig. 7b**,**c**). Analysis of the highest quartile of expressed genes revealed that the size of the NDR increased at S and M phases by ~220 base pairs and 270 base pairs, respectively, compared to G1 phase (**Supplementary Fig. 7b**). Moreover, this increase in the size of the NDR at S and M phases directly relates to the loss of the −2 and −1 nucleosome located upstream and at the TSS, respectively (**Supplementary Fig. 7b**,**c**). The NDR minima differed profoundly between G1, S and M phases, which directly correlates with the extent of loss of the −1 nucleosome that is, at G1 phase when the −1 nucleosome is present, the NDR minima are located at +230 base pairs. In contrast, when this nucleosome is completely absent at S phase, the NDR minima are now located at −50 base pairs relative to the TSS (**Supplementary Fig. 7b**,**c**).

To validate this change in the location of the NDR as the trophoblast stem cell cycles from G1 to M phase, we examined the distribution of histone H3 by analyzing our histone H3 ChIP-seq data (**Supplementary Fig. 3**). Mirroring the input nucleosome data, the depleted histone H3 region at G1 phase was located at +230 base pairs relative to the TSS, whereas at S and M phases, the region depleted in histone H3 was at the TSS (**Supplementary Fig. 3**).

We then investigated whether the marked increase in the size of the NDR for genes expressed at S and M phases is related to the unique chromatin organization required for transcription at these stages of the cell cycle or whether this size increase is an indirect consequence of passage through S phase. Following the profiles for the normalized input nucleosome tag count at each of the three stages of the cell cycle for the top 100 G1 > M, S > G1, and M > G1 expressed genes (as used in **Figs. 1** and **4**), all active genes exhibited a more extensive NDR at S phase, which was maintained at M phase, irrespective of which stage of the cell cycle they were more highly expressed (**Fig. 7d**–**f**). This was exemplified for G1 > M expressed genes because the TSS becomes more accessible to micrococcal nuclease digestion at S and M phases despite being more highly transcribed in G1 phase. These results show that the cell cycle and not transcription in itself is the major remodeler of chromatin at the TSS.

DISCUSSION

Our investigation of how histone H2A.Z is inherited given its importance in establishing an active transcriptionally poised state revealed (i) transctiption-independent major changes to the composition and abundance of histone H2A.Z–containing nucleosomes during and after DNA replication; (ii) dynamic genomic relocalization of histone H2A.Z to centromeric and subtelomeric regions at M phase; (iii) major cell cycle–dependent changes in the size and location of the NDR at the TSS occur mirroring the dynamic alterations in histone H2A.Z; (iv) heterotypic histone H2A.Z–H2A nucleosomes marking the TSS and CTCF binding sites but only at G1 phase; and (v) the location of CTCF protein binding sites change during the cell cycle.

The notable finding of this investigation is that all active genes, irrespective of which stage of the cell cycle they are more highly expressed in, exhibit the same following features as the cell cycle progresses from G1 phase to M phase: (i) an overall reduction in the amount of histone H2A.Z at the promoter, (ii) an increase of histone H2A.Z–H2A heterotypic nucleosomes upstream and downstream of the TSS, (iii) the loss of a heterotypic nucleosome from the TSS and (iv) an increase in NDR size. Given that these alterations to the NDR do not correlate with transcription level, our major conclusion is that the cell cycle is a major remodeler of the structure and composition of active chromatin.

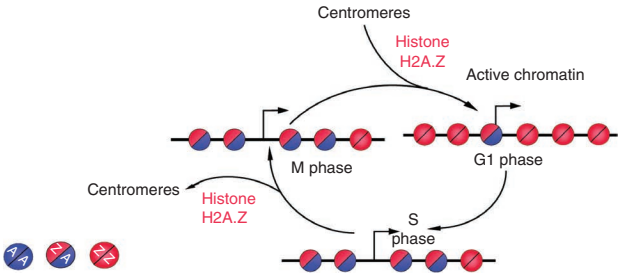

Figure 8 A model depicting the dynamic changes in histone H2A.Z at an active promoter throughout the cell cycle. Active genes in G1 phase have homotypic histone H2A.Z–containing nucleosomes immediately upstream and downstream of the TSS, with a heterotypic histone H2A.Z–H2A nucleosome located at the TSS. A, histone H2A; Z, histone H2A.Z. During DNA replication, homotypic histone H2A.Z nucleosomes become heterotypic and the heterotypic histone H2A.Z–H2A nucleosome at the TSS is lost. As cells progress to M phase, there is a net movement of histone H2A.Z to the centromere (and subtelomeric regions) preventing the reestablishment of homotypic nucleosomes at active promoters. Upon completion of mitosis, there is a redistribution of histone H2A.Z from the centromere back to active promoters to restore the original G1-phase active chromatin state.

The total amount of bulk histone H2A.Z in chromatin does not change during the cell cycle (**Supplementary Fig. 1b**), so why does histone H2A.Z become partially depleted at promoters as the trophoblast stem cell passes from G1 phase to M phase resulting in an increase in histone H2A.Z–H2A heterotypic nucleosomes? Given that the loss of histone H2A.Z at promoters is coincident with its gain at centromeric and subtelomeric regions, we propose that there is a dynamic net movement of histone H2A.Z from promoters to these repetitive DNA elements when they become functionally important. Our results are consistent with the model that upon completion of mitosis, histone H2A.Z is targeted back to promoters (**Fig. 8**).

The TSS is marked by a micrococcal nuclease–sensitive nucleosome, and it has been shown previously that this nucleosome comprises two histone variants, H3.3 and H2A.Z (ref. 7). Although it has been shown that this double-variant nucleosome isolated from cells was unstable[8], the structural basis for its instability remains unclear[9]. We demonstrated here that this unstable nucleosome located at the TSS is heterotypic in respect to histone H2A.Z, which may offer a molecular explanation for its instability. Based on the crystal structure of a homotypic histone H2A.Z–H2A.Z nucleosome, it has been predicted that the replacement of one histone H2A.Z with histone H2A will cause a major structural clash between their L1 loop regions, which is sufficient to destabilize it[9,18].

Genes active at S and M phases do not contain the heterotypic histone H2A.Z–H2A nucleosome at their TSS, so what might be the function of this special nucleosome for genes active at G1 phase? Given that we only observed a stable nucleosome located at the TSS for genes active at G1 phase (**Fig. 7d** and **Supplementary Fig. 7**), we propose that incorporation of only a single molecule of histone H2A.Z (together with histone H3.3 (ref. 7)) may be part of the

remodeling mechanism that enables this nucleosome to be disrupted to facilitate transcription. The function of this heterotypic nucleosome is replaced by a nucleosome containing histone H2A.Lap1 in the mouse testis[19].

Here we showed that the CTCF binding site is marked by a heterotypic histone H2A.Z–H2A nucleosome, which previously has been shown to be indexed by nucleosomes containing both histone H2A.Z and H3.3 (ref. 7). We therefore can conclude that a key feature of these unstable double-variant nucleosomes is that they are heterotypic in respect to histone H2A.Z. To our surprise this heterotypic nucleosome was present at G1 phase but not at S and M phases. We found that CTCF did not bind to a single site at G1 phase, whereas at M phase, when the histone H2A.Z–H2A nucleosome is absent, we observed a strong single peak of binding. This suggests that this heterotypic nucleosome may be inhibitory to CTCF binding, and the broad and symmetrical binding pattern observed at G1 phase (**Fig. 5b**) could be explained by the binding of CTCF to the edges of this heterotypic nucleosome in the linker DNA region, which is consistent with a previous study[13]. At M phase when this heterotypic nucleosome is no longer present, CTCF can bind to one central location. CTCF has been proposed to be a major player in regulating the architecture of the genome by mediating inter and intrachromosome interactions[14]. Our data showing that new CTCF binding sites appear at M phase compared to the G1 phase (**Fig. 5b**,**c**) indicates that major changes in the organization of the whole mouse genome occur during the cell cycle.

It has been hypothesized that the inheritance of an active epigenetic state during the cell cycle may provide transcriptional memory, that is, active marks established at G1 phase that remain at M phase may facilitate the rapid reestablishment of gene transcription after cell division[20]. Such a role has been postulated for histone H2A.Z (ref. 6). However, whereas our findings do not totally exclude this possibility, we showed that the abundance of histone H2A.Z changes at promoters and the centromere during the course of a cell cycle, which brings into question such a specific role. Indeed, it is emerging that histone post-translational modifications and other histone variants are restored slowly after DNA replication, and in some instances requiring more than one round of cell division to be fully reestablished[21–23]. It is attractive to speculate that the cell cycle–dependent increase in the accessibility of an active or poised TSS that we observed here could potentially provide the chromatin-based information needed for transcriptional memory.

METHODS

Methods and any associated references are available in the online version of the paper.

Accession code. Gene Expression Omnibus: GSE41091.

Note: Supplementary information is available in the online version of the paper.

ACKNOWLEDGMENTS

We thank M. Day (University of Sydney) for providing us with trophoblast stem cells and advice on their maintenance. We acknowledge the excellent high-throughput DNA sequencing service provided by our in house Biomolecular Research Service headed by S. Palmer. We thank D. Ryan for his help with the quantification of histone H2A.Z at the different stages of the cell cycle and H. French for early help in analyzing the microarray data. This work was supported by Australian National Health and Medical Research Council project grants to T.A.S. and D.J.T. (1009851), and M.N. and D.J.T. (1009850).

AUTHOR CONTRIBUTIONS

M.N. performed and helped design the experiments. J.A. carried out the cell-synchronization experiments. T.A.S. established the trophoblast stem cell system and performed the human U20S cell synchronization experiments. R.W. developed and performed data analysis of global mouse gene expression data. G.A.H. designed and contributed to interpretation of the analysis of the Illumina short read data. C.J. assisted with the design and executed the analyses of Illumina short read data. B.J.P. designed and contributed to the interpretation of the computational analysis of CTCF binding sites. D.J.T. conceived the project, helped design the experiments and wrote the manuscript.

COMPETING FINANCIAL INTERESTS

The authors declare no competing financial interests.

Published online at http://www.nature.com/doifinder/10.1038/nsmb.2424.
Reprints and permissions information is available online at http://www.nature.com/reprints/index.html.

1. Guillemette, B. & Gaudreau, L. Reuniting the contrasting functions of H2A.Z. *Biochem. Cell Biol.* **84**, 528–535 (2006).
2. Jiang, C. & Pugh, B.F. Nucleosome positioning and gene regulation: advances through genomics. *Nat. Rev. Genet.* **10**, 161–172 (2009).
3. Mavrich, T.N. *et al.* Nucleosome organization in the *Drosophila* genome. *Nature* **453**, 358–362 (2008).
4. Yadon, A.N. *et al.* Chromatin remodeling around nucleosome-free regions leads to repression of noncoding RNA transcription. *Mol. Cell. Biol.* **30**, 5110–5122 (2010).
5. Barski, A. *et al.* High-resolution profiling of histone methylations in the human genome. *Cell* **129**, 823–837 (2007).
6. Kelly, T.K. *et al.* H2A.Z maintenance during mitosis reveals nucleosome shifting on mitotically silenced genes. *Mol. Cell* **39**, 901–911 (2010).
7. Jin, C. *et al.* H3.3–H2A.Z double variant-containing nucleosomes mark 'nucleosome-free regions' of active promoters and other regulatory regions. *Nat. Genet.* **41**, 941–945 (2009).
8. Jin, C. & Felsenfeld, G. Nucleosome stability mediated by histone variants H3.3 and H2A.Z. *Genes Dev.* **21**, 1519–1529 (2007).
9. Henikoff, S. Labile H3.3+H2A.Z nucleosomes mark 'nucleosome-free regions'. *Nat. Genet.* **41**, 865–866 (2009).
10. Creyghton, M.P. *et al.* H2AZ is enriched at polycomb complex target genes in ES cells and is necessary for lineage commitment. *Cell* **135**, 649–661 (2008).
11. Jackson, V. & Chalkley, R. Histone synthesis and deposition in the G1 and S phases of hepatoma tissue culture cells. *Biochemistry* **24**, 6921–6930 (1985).
12. Faast, R. *et al.* Histone variant H2A.Z is required for early mammalian development. *Curr. Biol.* **11**, 1183–1187 (2001).
13. Fu, Y., Sinha, M., Peterson, C.L. & Weng, Z. The insulator binding protein CTCF positions 20 nucleosomes around its binding sites across the human genome. *PLoS Genet.* **4**, e1000138 (2008).
14. Millau, J.F. & Gaudreau, L. CTCF, cohesin, and histone variants: connecting the genome. *Biochem. Cell Biol.* **89**, 505–513 (2011).
15. Greaves, I.K., Rangasamy, D., Ridgway, P. & Tremethick, D.J. H2A.Z contributes to the unique 3D structure of the centromere. *Proc. Natl. Acad. Sci. USA* **104**, 525–530 (2007).
16. Rangasamy, D., Greaves, I. & Tremethick, D.J. RNA interference demonstrates a novel role for H2A.Z in chromosome segregation. *Nat. Struct. Mol. Biol.* **11**, 650–655 (2004).
17. Schones, D.E. *et al.* Dynamic regulation of nucleosome positioning in the human genome. *Cell* **132**, 887–898 (2008).
18. Suto, R.K., Clarkson, M.J., Tremethick, D.J. & Luger, K. Crystal structure of a nucleosome core particle containing the variant histone H2A.Z. *Nat. Struct. Biol.* **7**, 1121–1124 (2000).
19. Soboleva, T.A. *et al.* A unique H2A histone variant occupies the transcriptional start site of active genes. *Nat. Struct. Mol. Biol.* **19**, 25–30 (2012).
20. Probst, A.V., Dunleavy, E. & Almouzni, G. Epigenetic inheritance during the cell cycle. *Nat. Rev. Mol. Cell Biol.* **10**, 192–206 (2009).
21. Jansen, L.E., Black, B.E., Foltz, D.R. & Cleveland, D.W. Propagation of centromeric chromatin requires exit from mitosis. *J. Cell Biol.* **176**, 795–805 (2007).
22. Scharf, A.N., Barth, T.K. & Imhof, A. Establishment of histone modifications after chromatin assembly. *Nucleic Acids Res.* **37**, 5032–5040 (2009).
23. Xu, M., Wang, W., Chen, S. & Zhu, B. A model for mitotic inheritance of histone lysine methylation. *EMBO Rep.* **13**, 60–67 (2012).

ONLINE METHODS

Cell culture and cell-cycle synchronization. Mouse trophoblast stem (TS) cells were cultured as originally described[24]. To synchronize TS cells at the G2-M phase boundary, cells were treated with nocodazole (40 ng/ml) for 7 h before collection. This concentration was chosen after an extensive analysis to determine the minimum concentration required to synchronize cells without any adverse effects to the cell cycle or subsequent differentiation. To synchronize TS cells in S phase, TS cells were washed after treatment with nocodazole (40 ng/ml) an allowed to grow for an additional 7 h in drug-free fresh TS cell medium. To synchronize TS cells at the G1-S phase boundary after nocodazole treatment, TS cells were washed and grown for 3 h in fresh medium. Hydroxyurea (5 mM) was then added, and the cells were grown for an additional 5 h before they were collected. To synchronize U2OS cells at G2-M phase, cells were treated with nocodazole (50 ng/ml) for 16 h before collection. To arrest these cells at the G1-S phase boundary, they were treated with hydroxyurea (2 mM) for 16 h before collection.

Chromatin preparation. Mononucleosomes were prepared essentially as we recently described[19]. TS cells or U2OS cells were grown in 150-mm dishes containing 2–5 × 10^7 cells per dish. Cells were fixed for 15 min at room temperature in 10 ml of fresh DMEM with 10% (v/v) FBS in the presence of 1.5% (v/v) formaldehyde. Cross-linking was stopped by adding glycine solution to a final concentration of 0.125 M. Fixed cells were washed three times with ice-cold PBS (20 ml). Cells were then scraped into ice-cold PBS (15 ml), containing 0.05% (v/v) Triton X-100. Cells were then pelleted at 900*g* for 5 min at 4 °C. The cell pellet was resuspended with 2 ml of buffer I (25 mM Hepes pH 7.6, 15 mM NaCl, 10 mM KCl, 2 mM $MgCl_2$, 0.2% (v/v) NP-40, 1 mM EDTA, 0.5 mM EGTA, 0.5 mM DTT, 0.2 mM PMSF and Roche EDTA-free protein inhibitor cocktail) and incubated on ice for 10 min. Two milliliters of buffer II (0.6 M sucrose, 15 mM Hepes pH 7.6, 120 mM KCl, 15 mM NaCl, 2 mM $MgCl_2$, 0.2% (v/v) NP-40, 1 mM EDTA, 0.5 mM EGTA, 0.5 mM DTT, 0.2 mM PMSF and Roche EDTA-free protein inhibitor cocktail) was added and the suspension was incubated for a further 10 min. Nuclei were released by 20 strokes with a Dounce homogeniser type B and pelleted by centrifugation (40 min at 5,000*g*) through a 8 ml sucrose cushion containing buffer III (1.2 M sucrose, 60 mM KCl, 15 mM Hepes pH 7.6, 15 mM NaCl, 2 mM $MgCl_2$, 1 mM EDTA, 0.5 mM EGTA, 0.5 mM DTT, 0.2 mM PMSF and Roche EDTA-free protein inhibitor cocktail). The supernatant was carefully removed and the nuclei pellet was resuspended in 1 ml of micrococcal digestion buffer (50 mM Tris-HCl pH 7.6 and 3mM $CaCl_2$) and passed 10 times through a size 29-gauge needle. The nuclear extract was digested for 30 min at 37 °C with micrococcal nuclease (New England Biolabs; 2 units per 330 µl of extract) to obtain chromatin comprising mostly mononucleosomes. The reaction was stopped by adding 15 µl of 100 mM EDTA. The digested nuclear extract was centrifuged at 10,000*g* for 5 min. The supernatant containing mononucleosomes (S1) and the pellet (which was resuspended in 500 µl of dialysis buffer (10 mM Tris-HCl pH 7.6, 1 mM EDTA and 0.5 mM EGTA) were dialyzed independently overnight at 4 °C. The dialyzed resuspended pellet was centrifuged at 10,000*g* for 10 min and the supernatant (S2), containing short chromatin fragments primarily mononucleosomes, was mixed with S1. The combined S1 and S2 supernatants were dialyzed against 10 mM Tris-HCl pH 7.6, 1 mM EDTA, 0.5 mM EGTA and 4% (v/v) glycerol, aliquoted and stored at −80 °C. Antibodies used for the western blot analysis are described in **Supplementary Note**.

ChIP and sequential ChIP assays, preparation of ChIP-seq DNA libraries and data analysis. ChIP assays, preparation of ChIP-seq libraries and DNA sequence data analysis were carried out as we recently described[19]. Chromatin immunoprecipitations were performed with the following modifications. Anti–histone H2A.Z antibodies[25] (5 µg; in-house), anti–histoneH3 antibodies (5 µg; ab1791; Abcam), anti-CTCF antibodies (7 µg; ab70303; Abcam) or control mock IgG (10 µg) were added to 40 µl of Dynabeads Protein A or Protein G (Dynal Biotech ASA) and incubated for 1 h at room temperature, followed by two washes with 200 µl PBS, 0.01% (v/v) Tween 20. We combined 100 µg of chromatin with 1 ml of radioimmunoprecipitation assay buffer (RIPA) buffer (140 mM NaCl, 10 mM Tris-HCl pH 8.0, 1 mM EDTA, 1% (v/v) Triton X-100, 0.1% (w/v) SDS, 0.1% (w/v) sodium deoxycholate and 1 mM PMSF), mixed with antibodies and incubated overnight at 4 °C. Bound chromatin was subsequently washed (10 min per wash) three times with RIPA buffer, three times with RIPA buffer plus 0.36 M NaCl, once with LiCl buffer (250 mM LiCl, 10 mM Tris-HCl pH 7.6, 1 mM EDTA, 0.5% (v/v) NP-40 and 0.5% (w/v) sodium deoxycholate, and finally twice with TE buffer (10 mM Tris-HCl pH 7.6 and 1 mM EDTA). Washed beads were resuspended in 90 µl of cold TE buffer and treated with 1 µl (0.5 mg/ml) RNase A (Roche) for 30 min and then with 0.5 mg per ml proteinase K (Invitrogen) for 4 h at 65 °C followed by 1 h at 72 °C to reverse cross-linking. An aliquot of the original input chromatin was processed in parallel. DNA from the samples was recovered using AMPure XP beads (Agencourt) according to the manufacturer's protocol. Sequential histone H2A.Z ChIP–histone H2A reChIP was carried out as described previously with minor modifications[26]; after the final ChIP wash, chromatin complexes were eluted twice in 100 µl of 10 mM DTT at 37 °C for 30 min and diluted 20 times with RIPA buffer. Eluates were reimmunoprecipitated with the second primary antibody to histone H2A (5 µg) (ab18255; Abcam), as described above. Although it is not possible to determine the efficiency of the histone H2A reChiP procedure using different histone antibodies because of their different affinities for their antigen, we performed the reChiP using antibodies to histones H3 and H2A.Z, respectively, and found in both cases we could recover ~50% of the initial histone H2A.Z ChIP DNA (data not shown).

Libraries for ChIP sequencing of DNA were prepared using ChIP-Seq Sample Prep Kit (Illumina) according to the manufacturer's protocol. Quality and concentration of the libraries were assessed on Agilent Technologies 2100 Bioanalyzer and using quantitative PCR with adaptor specific primers (ABI Prism 7900HT) according to Illumina's recommendations. DNA from input nucleosomes, histone H2A.Z ChIP and histone H2A.Z ChIP–histone H2A reChIP experiments was sequenced using the Genome Analyzer 2X (Illumina) using 75-base-pair single-end reads. CTCF and histone H3 ChIP-seq libraries were sequenced on the HiSeq 2000 (Illumina) in paired-end mode (100 base pairs).

ChIP-seq data are presented as the sum of totals reads per base pair per million of total mapped reads (reads per million mapped, RPM). For histone H2A.Z ChIP experiments, the total number of mapped single end reads were 20, 15 and 15 million for G1, S and M phases, respectively; for histone H2A.Z ChIP–histone H2A reChIP experiments, the single-end reads were 22, 19 and 19 million for G1, S and M phases, respectively; for input nucleosomes, the mapped read counts were around 10 million for all stages of the cell cycle; for histone H3 ChIP experiments, the mapped read counts were 26, 17 and 44 million for G1, M and S phases, respectively.

A custom pipeline for processing Illumina sequence data was implemented using PyCogent 1.5.dev as we described previously[19]. The pipeline, to which we refer as ChipPy, was implemented in the Python programming language (version 2.7) as an extension of the PyCogent genomic biology library. Sequenced reads were cleaned with FASTX-Toolkit (http://hannonlab.cshl.edu/fastx_toolkit/index.html) and aligned to the mouse genome (Ensembl release 62) with BWA v0.5.9 (ref. 27).

To perform histone H2A.Z ChIP assays on specific genes to validate our approach and interpretation of the ChIP-seq data, DNA was analyzed by real-time quantitative PCR (ABI Prism 7900HT) using SYBR Green PCR master mix and standard settings (Applied Biosystems). PCR was performed in triplicates and serial dilutions of purified input DNA were measured together with the immunoprecipitated DNA samples. Histone H2A.Z ChIP signals were normalized for input signals (ΔCt) and corrected for values obtained with non-immune control antibodies (ΔΔCt). The relative sample enrichment was calculated with the following formula $2^{-\Delta\Delta Ct}$. To perform histone H2A.Z ChIP and H2A reChIP assays on repetitive DNA elements, ChIP DNA libraries were prepared as described above. The DNA concentration of each individual library was measured by quantitative PCR with adaptor-specific primers and adjusted accordingly to the same final concentration (10 pM). Each ChIP library was then used for quantitative PCR using DNA sequence specific primers (**Supplementary Table 1**). Experiments were performed with two biological replicates, each in triplicate.

CTCF ChIP-seq. The 100-base-pair paired end CTCF ChIP-seq was performed using standard protocols on the Illumina Hi-seq platform. Palindromic adaptor trimming was performed using Trimmomatic (http://usadellab.org/cms/) and reads were mapped using Bowtie 2 (ref. 28) with default mapping parameters. Total mapped read numbers were 71 million (G1 phase), 63 million (M phase) and 19 million (S phase). Median insert size was 153 base pairs (M phase), 153 base pairs (G1 phase) and 111 base pairs (S phase). Duplicate reads were retained. Reads were extended to full fragments; then coverage was computed. CTCF peaks

doi:10.1038/nsmb.2424

were defined by >10 reads and >50-base-pair (bp) width, M phase samples showed 37% overlap of peaks with G1 phase samples (38% with duplicate reads removed; a more stringent definition of >50 reads and >100-bp width showed 13% overlap). Per-base coverage, normalized to total mapped reads (RPM), of CTCF ChIP-seq and ChIP-reChIP histone H2A.Z over 2,000-bp regions anchored at Encode-annotated CTCF sites (Encode MEL cell line) was plotted.

Expression analysis. Expression analysis is described in the **Supplementary Note**.

24. Tanaka, S., Kunath, T., Hadjantonakis, A.K., Nagy, A. & Rossant, J. Promotion of trophoblast stem cell proliferation by FGF4. *Science* **282**, 2072–2075 (1998).
25. Rangasamy, D., Berven, L., Ridgway, P. & Tremethick, D.J. Pericentric heterochromatin becomes enriched with H2A.Z during early mammalian development. *EMBO J.* **22**, 1599–1607 (2003).
26. Soutoglou, E. & Talianidis, I. Coordination of PIC assembly and chromatin remodeling during differentiation-induced gene activation. *Science* **295**, 1901–1904 (2002).
27. Li, H. & Durbin, R. Fast and accurate short read alignment with Burrows-Wheeler transform. *Bioinformatics* **25**, 1754–1760 (2009).
28. Langmead, B. & Salzberg, S.L. Fast gapped-read alignment with Bowtie 2. *Nat. Methods* **9**, 357–359 (2012).